Cell, Vol. 95, 541–552, November 13, 1998, Copyright ©1998 by Cell Press

Crystal Structure and ATPase Activity of MutL: Implications for DNA Repair and Mutagenesis

Changill Ban and Wei Yang*
Laboratory of Molecular Biology
National Institute of Diabetes
and Digestive and Kidney Diseases
National Institutes of Health
Bethesda, Maryland 20892

Summary

MutL and its homologs are essential for DNA mismatch repair. Mutations in genes encoding human homologs of MutL cause multiorgan cancer susceptibility. We have determined the crystal structure of a 40 kDa N-terminal fragment of *E. coli* MutL that retains all of the conserved residues in the MutL family. The structure of MutL is homologous to that of an ATPase-containing fragment of DNA gyrase. We have demonstrated that MutL binds and hydrolyzes ATP to ADP and Pi. Mutations in the MutL family that cause deficiencies in DNA mismatch repair and a predisposition to cancer mainly occur in the putative ATP-binding site. We provide evidence that the flexible, yet conserved, loops surrounding this ATP-binding site undergo conformational changes upon ATP hydrolysis thereby modulating interactions between MutL and other components of the repair machinery.

Introduction

Repair of DNA base pair mismatches ensures genomic stability in virtually all living organisms (reviewed by Modrich, 1991; Kolodner, 1996). The primary sources of mismatches are mispairing during DNA replication and various DNA recombination events. Failure to correct such mismatches results in an increased mutation rate and instability of genomic DNA, such as microsatellite instability and postmeiotic segregation (PMS). As Loeb and Nowell suggested 20 years ago (Loeb et al., 1974; Nowell, 1976), genetic destabilization predisposes a cell to malignant changes. Humans and mice inheriting defective genes encoding DNA mismatch repair machinery are indeed susceptible to development of cancers in various organs, including the colorectum, endometrium, ovary, stomach, small intestine, kidney, and ureter, collectively called hereditary nonpolyposis colorectal cancer (HNPCC) (Modrich and Lahue, 1996; Peltomäki and Vasen, 1997). Microsatellite instability is also linked to a significant fraction of sporadic tumors.

The MutS and MutL proteins comprise the best characterized mismatch repair system, and homologs of these proteins have been found in prokaryotes, archaebacteria, yeast, *Xenopus laevis*, *Drosophila melanogaster*, and mammals (Modrich and Lahue, 1996). In vitro reconstituted repair machinery from *E. coli* provides an example of how mismatches are repaired in a strand-specific manner (Lahue et al., 1989). Initiation of mismatch repair requires MutS, MutL, MutH, and ATP to introduce an incision in the strand that is targeted for repair (reviewed by Modrich, 1991; Modrich and Lahue, 1996). MutS recognizes a mismatched base pair as well as an insertion or deletion of one to four nucleotides in one strand. MutS is also an ATPase that translocates along DNA and promotes DNA loop formation (Allen et al., 1997). In the presence of ATP, MutS and MutL together activate MutH, which is a latent sequence- and methylation-specific endonuclease. If the mismatch occurs as a result of a replication error, MutH cleaves 5′ to the sequence d(GATC) in the newly synthesized and unmethylated daughter strand (Lahue et al., 1989). The template strand in wild-type *E. coli* is methylated and therefore resistant to MutH cleavage. MutS and MutL are also required in the subsequent DNA repair step to activate UvrD helicase to unwind the DNA (Dao and Modrich, 1998; Yamaguchi et al., 1998), making it a substrate for single strand–specific exonucleases, which remove nucleotides from the nick made by MutH to beyond the mispaired bases (Cooper et al., 1993; Grilley et al., 1993). MutS and MutL may also play a role in selecting DNA polymerase III holoenzyme to fill the gap in the final stage of mismatch repair.

In eukaryotes, MutL homologs are designated as MLH and PMS. The *pms* gene was named for the phenotype of postmeiotic segregation before it was cloned and found to be homologous to MutL (Kramer et al., 1989). MutS homologs are best known as MSH proteins and recognize heterologies in a DNA duplex, such as mismatches (reviewed by Kolodner, 1996; Modrich and Lahue, 1996). Similar to the *E. coli* proteins, eukaryotic MutS homologs, MLHs, and PMSs are essential for DNA mismatch repair. Mutations in genes encoding human *MLH1* account for over 50% of the reported HNPCC cases, followed by mutations in *MSH2* (~40%), *PMS1*, and *PMS2* genes (Peltomäki and Vasen, 1997). Mutations of *MLH1* have recently been identified in human leukemia and lymphoma cell lines as well (Hangaishi et al., 1997). Although the linkage between cancer susceptibility and DNA mismatch repair has been established, the relationship between DNA repair proteins and tissue-specific development of cancer is unclear. For example, null mutation of *PMS2* in mice resulted in male infertility among other phenotypes (Baker et al., 1995); knockout mice defective in both alleles of *MSH2* are viable and prone to lymphomas but not colon cancer (de Wind et al., 1995). MutL homologs in eukaryotes, notably in humans, are clearly essential for normal cell growth. However, the exact activities of these proteins have not been determined.

All members of the MutL family have a conserved region of ~300 residues at their N terminus (Figure 1) and a rather diverse C-terminal region of 300 to 500 residues. They often form homo- or heterodimers in solution (Grilley et al., 1989; Pang et al., 1997). The majority of the reported mutations with dominant mutator phenotypes in *E. coli* MutL (Aronshtam and Marinus, 1996) are

* To whom correspondence should be addressed (e-mail: wei.yang@nih.gov).

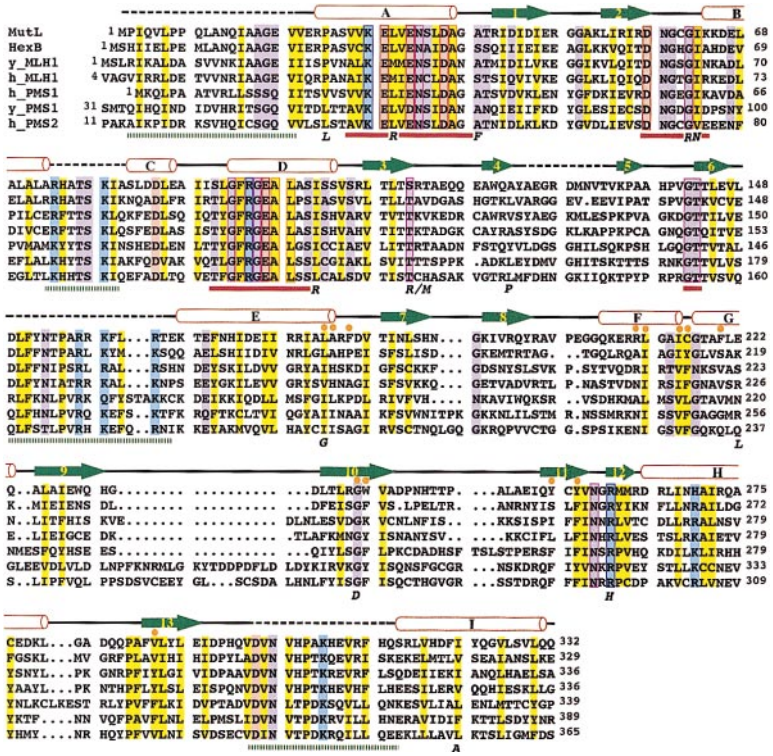

Figure 1. Sequence Alignment of the MutL Family

Structure-based sequence alignment of the conserved N-terminal region in the MutL family. MutL is from *E. coli*; HexB is from *S. Pneumoniae*; MLH and PMS from both yeast and human are included. Secondary structures are indicated over the sequence alignment, rods for α helices, arrows for β strands, and dashed lines for disordered loops. Conserved hydrophobic residues are shaded in yellow, basic in blue, acidic in red, and others in purple. The conserved residues in the ATP-binding pockets are outlined. Four ATP-binding motifs, which are common among NgyrB, Hps90, and MutL, are underlined in red. Four sequence segments, which are conserved in the MutL family but form disordered loops in the LN40 structure, are underlined in green dashes. Residues located at the domain interface are indicated by orange balls. Missense mutations found in human MLH1 from HNPCC family are shown in italic letters under the sequence alignment.

within the conserved N-terminal region; more than 50% of missense mutations found in human MLH1 of HNPCC (Peltomäki and Vasen, 1997) are also within the equivalent conserved region. Attempts to assign simple biochemical activities to MutL have been unsuccessful even in *E. coli* where each component involved in DNA mismatch repair has been identified. *E. coli* MutL has been proposed to mediate the interaction between the endonuclease MutH and the mismatch recognition protein MutS (Grilley et al., 1989; Lahue et al., 1989). MutS and MutL were shown to be associated in heteroduplex loop formation by electron microscopy (Allen et al., 1997). Addition of MutL also dramatically expanded the region protected by MutS in a DNA footprinting analysis (Lahue et al., 1989). However, it has not been shown whether MutL directly interacts with DNA. Alteration in the DNA footprint could result from interactions between MutS and MutL. Evidence of a physical interaction between MutL and UvrD has been reported recently (Hall et al., 1998). It is unclear, however, whether MutL interacts with MutH and how MutL switches from activating MutH to recruitment of the helicase to a repair site.

MutL and its homologs have not attracted as much scrutiny as the MutS family even though mutations in the MutL and MutS families display similar phenotypic defects. The primary reason for the shortage of attention to the MutL family is due to a lack of an identified activity of the MutL family. With little biochemical data on the functions and no structural information, it has been difficult even to formulate questions to address. We have determined and report here the crystal structure of the conserved N-terminal fragment of *E. coli* MutL (LN40). We show that this conserved fragment binds to DNA and can activate MutH in DNA repair. In addition, we demonstrate that MutL is an ATPase and that ATP binding triggers conformational changes in MutL. The ATP-dependent conformational changes are likely to regulate interactions of MutL with other components in the DNA repair machinery.

Results and Discussion

LN40 Binds DNA and Can Activate MutH

E. coli MutL, a 70 kDa protein, is cleaved by thrombin to an N-terminal 40 kDa fragment (LN40, residue 1–349) and a C-terminal 30 kDa fragment (LC30, residues 350–615). LN40 contains all of the conserved residues characteristic of the MutL family. In contrast to intact MutL, which forms a dimer, LN40 is monomeric in solution as judged by size exclusion chromatography and equilibrium ultracentrifugation (data not shown). This finding is consistent with reports that the C-terminal regions mediate dimerization in both *E. coli* MutL (Drotschmann et al., 1998) and its eukaryotic homologs (Pang et al., 1997).

A 110 bp DNA heteroduplex (Mis-110) was constructed, which contains a G-T mismatch near one end and an unmethylated GATC sequence near the other (Figure 2a). A DNA mobility shift assay shows a discrete band of LN40-DNA complex indicating that LN40 binds to Mis-110 (Figure 2b) as do both MutS and MutH, although MutS and MutH interact with Mis-110 more strongly (data not shown). Not only is DNA binding by MutL relatively weak, but LN40 also appears to aggregate on DNA resulting in a slowly migrating DNA–protein complex that remains close to the sample well (Figure 2b). To determine if DNA binding by LN40 is mismatch-dependent, the DNA mobility shift assay was performed

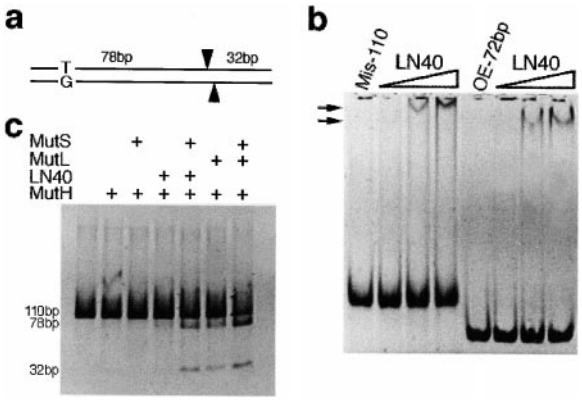

Figure 2. DNA Binding and Cleavage by MutL

(a) Mis-110, a 110 bp DNA heteroduplex with a G-T mismatch near one end. Arrows mark the unmethylated GATC sequence where MutH cleaves.

(b) DNA mobility shift by LN40. Hetero- or homoduplex DNA, (Mis-110 and OE-72), was incubated with LN40. The molar ratios of LN40 to DNA were 1, 3, and 5. Arrows point to the bands of DNA associated with LN40.

(c) Stimulation of Mis-110 cleavage by MutH in the presence of ATP. Presence of each protein is indicated by a + sign above each lane.

with a 72 bp homoduplex of sequence unrelated to Mis-110. LN40 also forms a complex with this shorter DNA, which migrates faster than that with Mis-110 (Figure 2b). These results indicate that LN40 binds to double-stranded DNA in a sequence and mismatch-independent manner. When intact MutL is mixed with DNA, both protein and DNA are retained in the sample wells (data not shown).

After confirming that MutS and MutL can activate MutH to cleave both strands of Mis-110 at the GATC sequence in the presence of ATP (Figure 2c), we find that LN40 is able to replace MutL in activating MutH using this assay system (Figure 2c). The level of MutH activation using LN40 is lower compared with MutL. Nevertheless, it indicates that the N-terminal 349 residues of MutL contain all of the elements necessary for interacting with DNA and for activation of MutH in the presence of MutS and ATP.

The Crystal Structure of LN40

The crystal structure of LN40 was determined by the SIRAS method and refined at 2.9 Å resolution (Table 1). LN40 is composed of two α/β domains. The first domain (residues 20–200) resembles a flattened rectangular box with an eight-stranded mixed β sheet forming one large flat surface and five α helices forming the opposite surface (Figure 3a). The topology of this domain can be characterized as three repeats of a helix-turn-β hairpin. In the second repeat, however, additional helices are found and the β hairpin folds into a Greek key configuration (Figure 3b). The second domain (residues 224–331) is an α/β barrel made of five mixed strands and two parallel helices. This α/β barrel contains an unusual left-handed crossover of strand-helix-strand, which has only been observed in a few proteins (see discussion later). Each domain in LN40 is stabilized by a hydrophobic core. The two domains are linked by two short helices to give LN40 an elbow-like appearance (Figure 3a). The interface between the two domains buries $\sim$1000 Å^2 of surface area and is dominated by aromatic and aliphatic residues (Figure 1). Most of the conserved residues, although dispersed in the primary sequence, are clustered in two exposed patches, a large region in the first domain and a smaller region in the second domain, facing each other inside the elbow (Figures 3a and 3c). Including the N and C termini, there are six disordered regions, four of which contain conserved sequences (Figure 1).

Structural Similarity Among MutL, DNA Gyrase, and Hsp90

It was reported recently that MutL may belong to a newly identified ATP-binding family that is characterized by three conserved sequence motifs and includes DNA gyrase, Hsp90, MutL and homologs, type II typoisomerases, and bacterial histidine kinase (Bergerat et al., 1997; Mushegian et al., 1997). The crystal structures have been reported for a two-domain ATPase–containing fragment of DNA gyrase (NgyrB) complexed with ADPnP (5′-adenylyl-β-γ-imidotriphosphate), a single ATP/ADP-binding domain from both yeast and human Hsp90, and the same domain of human Hsp90 complexed with an antitumor agent, geldanamycin (Prodromou et al., 1997a, 1997b; Stebbins et al., 1997). Structural similarity between gyrase and Hsp90 has been noted (Prodromou et al., 1997a). Comparison of the structures of LN40, NgyrB, and Hsp90 reveals extensive similarity (Figure 4a). The first domains of LN40 and NgyrB have essentially the same topology as the ATP/ADP-binding domain of Hsp90. The three conserved sequence motifs define an ATP-binding pocket in both NgyrB and Hsp90 (Figure 4b). This ATP-binding pocket entirely overlaps with the region in the first domain of LN40 that is conserved throughout the MutL family (Figure 1 and Figure 4).

The structural similarity between LN40 and NgyrB is even more extensive. Each domain of LN40 can be superimposed onto those in NgyrB with an RMS deviation of 2.0 Å including all main chain atoms for over 100 pairs of residues (Figure 4c). Interestingly, the eight-stranded β sheet and helix E seem to be better superimposed than helices A, B, and D (Figure 4c), which include most of the three conserved ATP-binding sequence motifs. The differences in helices A, B, and D probably reflect structural flexibility of this region, which shows large conformational changes upon ligand binding as observed in NgyrB and Hsp90 (see discussion later). The major difference between LN40 and NgyrB is the relative orientation of the two domains, which differs by 38° (Figure 4a). This difference could be the result of different protein sequences, the presence or absence of ATP, or crystal lattice contacts. The relatively small and hydrophobic interface between the two domains in LN40 poses little barrier for them to reorient. A structure-based sequence alignment of LN40 and NgyrB reveals greater than 30% similarity (Figure 4d), indicating that they are likely to have evolved from a common ancestor.

MutL Binds ADP, ATP, and ADPnP

MutL and LN40 binding of nucleotide was determined based on the increase of the UV absorption ratio at 260

Table 1. Summary of Crystallographic Data

Space group	$I2_12_12_1$ (two molecules per asymmetric unit)		
Crystals	Native 1	EMP	Native 2
Unit cell (Å)	87.2, 93.5, 221.2	87.6, 94.1, 221.4	87.2, 93.2, 221.7
Resolution limit* (Å)	3.0 (3.1–3.0)	2.7 (2.8–2.7)	2.7 (2.8–2.7)
Completeness* (%)	91.9 (81.2)	94.8 (80.7)	96.5 (84.6)
R_{rmerge}* (%)	7.2 (43.1)	7.2 (61.9)	7.4 (69.6)
R_{iso} (F)		14.1% (20.0–3.0 Å)	
Phasing power		1.32 (15.0–3.0 Å)	
Figure-of-merit		0.319 (15.0–3.0 Å)	
Refinement			
Protein atoms			4252
Solvent atoms			57
Unique reflections			19961 (20–2.9 Å)
R and (¶FreeR)			24.8% (29.6%)
RMS bond length			0.005 Å
RMS bond angle			1.221°

EMP stands for ethyl mercury phosphate.
Rmerge = $\Sigma_h\Sigma_i|I_{hi} - \langle I_h\rangle|/\Sigma\langle I_h\rangle$; Riso = $\Sigma||Fp| - |Fph||\Sigma|Fp|$.
Phasing power = $\langle|Fh|\rangle$/RMS (ϵ), that is the mean amplitudes calculated from the heavy-atom model divided by the lack of closure error.
$R = \Sigma||F_{obs}| - |F_{calc}||/\Sigma||F_{obs}|$; ¶FreeR is monitored with 5% of the reflection data excluded from refinement.
*data of the last resolution bin is shown in parenthesis.

nm versus 280 nm. MutL and LN40 were incubated with ADP, ATP, or ADPnP, then purified over a size-exclusion column. The UV absorption ratio at 260 nm versus 280 nm increases from 0.49 for MutL to 0.81 for the MutL-ADPnP complex and from 0.79 to 1.23 in the case of LN40. MutL and LN40 show different increments of absorption at 260 nm depending on the ligands. The ADPnP complexes have the highest ratio, the ATP complexes slightly lower, while the ADP complexes have a ratio between the apo-protein and the ADPnP complex. The differences in the UV absorption ratios probably reflect different dissociation constants of the ligands and that triphosphate binds better than diphosphate.

Using the theoretically calculated molar extinction coefficient of each protein and nucleotide and assuming that they are insensitive to the protein-nucleotide association, a nucleotide to protein molar ratio of 1.4:1 for the MutL-ADPnP complex and 1.1:1 for the LN40-ADPnP complex have been deduced from the UV absorption ratios. These ratios, which are close to 1:1, indicate that the nucleotide specifically binds to MutL and LN40 and not to a minor contaminant.

ATP-Binding Site in NgyrB, Hsp90, and LN40

Four sequence motifs (I-IV) are conserved among DNA gyrase, Hsp90, and MutL (Figure 4d). The first three motifs, EXXXNXXD, DXGXG, and GXXGXG/A, have been identified by sequence analyses (Bergerat et al., 1997; Mushegian et al., 1997). We have identified a new motif, Motif IV of Gly-Thr sequence, based on sequence, structural, and functional conservation. Motifs I, II, and IV in LN40 are structurally homologous to those in NgyrB and Hsp90 (Figure 4a). Most of the residues conserved in the MutL family are found on these four motifs (Figure 1), including E29, N33, D36, and A37 on αA, D58 to I63 on β2 and the following loop, and G142 and T143 on β6 (named as in *E. coli* MutL) and are positioned to directly interact with ATP when compared with NgyrB-ADPnP complex (Figures 4b). Other conserved residues in these motifs seem to be important for maintaining the structural integrity of the ATP-binding site, such as S112, whose hydroxyl group makes hydrogen bonds to both the amide nitrogen and the carbonyl oxygen of I63.

Motif III and residues preceding it show many structural variations. In NgyrB, this region assumes an extended conformation and forms extensive interactions with ADPnP. Based on its location and function, this loop has been referred to as the lid of the ATP pocket. The conserved Gly residues of Motif III (GXXGXG/A) make hydrogen bonds to the phosphate-moiety of ADPnP. Lys-103 and Tyr-109 in NgyrB also located on this ATP lid and make direct hydrogen bonds to the β-phosphate and N3 of adenine, respectively. The corresponding region in the ATP/ADP-binding domain of Hsp90 also forms a loop, but it is oriented differently (Figure 4a) and interacts with the nucleotide less extensively than that in NgyrB. This loop undergoes conformational changes in apo- versus ATP/ADP-bound forms in yeast Hsp90 (Prodromou et al., 1997a, 1997b). Its conformation also depends on ligands as well as crystal environment in both DNA gyrase (Lewis et al., 1996) and Hsp90 (Prodromou et al., 1997a, 1997b; Stebbins et al., 1997). The equivalent region in LN40 (residues 74–98) is partially disordered without ligand and points away from the ATP-binding pocket (Figures 4a and 4c). Motif III in LN40 (residues 93–98) assumes a helical conformation (the N-terminal half of αD) and blocks the ATP-binding site with the conserved R95 occupying the pocket for the adenine base (Figure 4b). Thus, helix D must undergo conformational changes in order to make the ATP-binding site available for the nucleotide.

In the NgyrB-ADPnP complex, the γ-phosphate is stabilized by residues Q335 and K337 from the second domain. The ATP/ADP-binding domain of Hsp90 lacks the second domain, and the γ-phosphate in the crystal structure is disordered. This ATP/ADP-binding fragment of Hsp90 has no ATPase activity. There is no conserved QXK sequence in the second domain of LN40. However, N302 and K307, which are conserved in the MutL family,

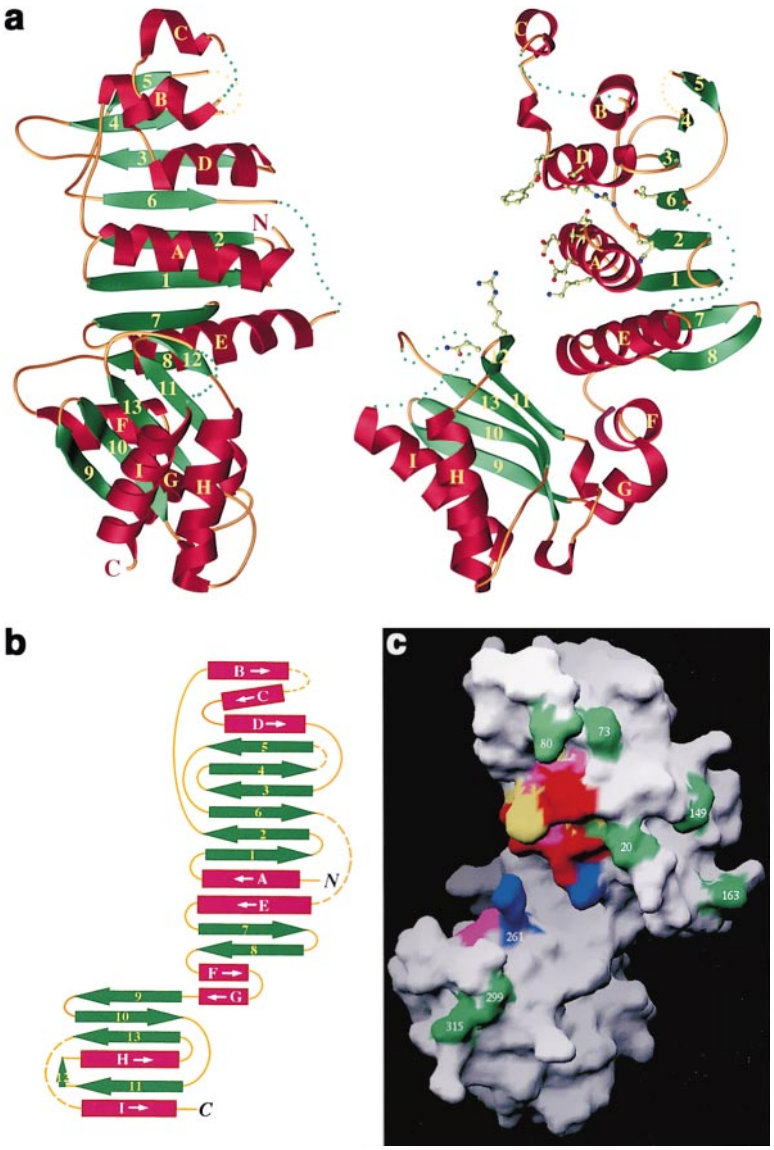

Figure 3. Crystal Structure of LN40

(a) Orthogonal views of LN40 in ribbon diagram. β strands are shown as green arrows, α and 3_{10} helices as red coils, and loops as yellow lines. In one of the views, conserved residues in the putative ATP-binding sites are shown in ball-and-stick. The disordered, yet conserved, loops are illustrated as green dotted lines.

(b) Topology of LN40. Secondary structures are labeled. Four internal disordered loops are shown as dashed lines.

(c) Molecular surface of LN40 shows the two solvent-exposed patches of conserved residues. The color scheme for conserved residues matches that in Figure 1. The green patches represent the ends of disordered yet conserved loops.

are in the equivalent loop to where QXK is in NgyrB and may play a role in stabilizing the γ-phosphate. In addition, the second domain of LN40 contains an NGR sequence (residues 259–261), which is conserved throughout the MutL family. R261 of the conserved NGR motif extends toward the ATP pocket in the first domain (Figure 2a). Mutation of the R261 equivalent in human MLH1 from Arg to His results in HNPCC (Peltomäki and Vasen, 1997). It is inviting to speculate that R261 may be the Arg that stabilizes the γ-phosphate in NTP binding (Vale, 1996).

MutL, DNA Gyrase, and EF-G Share an Unusual Left-Handed βαβ Fold

The program DALI (Holm and Sander, 1993) was used to search the Brookhaven Protein Database for structures similar to that of LN40 and indicated that the second domain of LN40 resembles a domain in elongation factor G protein (EF-G) (Ævarsson et al., 1994; Czworkowski et al., 1994), as does the second domain of NgyrB (Figure 5). EF-G comprises five domains and is a GTP-dependent ribosomal translocase. The overall structure of EF-G mimics the EF-Tu and tRNA complex. The domain in EF-G that is similar to LN40 interacts with the same portion of the ribosome as the anticodon loop of a tRNA. The similar domain in NgyrB contributes to ATP binding and directly interacts with the γ-phosphate. This domain, common among LN40, EF-G, and gyrase, has a rather unusual βαβ topology with a left-handed crossover connection (β11, β13, and αH in LN40) (Figure 5).

A recently determined crystal structure of RNase P protein (Stams et al., 1998) has a similar fold as found in EF-G, MutL, and DNA gyrase. Based on the limited finding that RNaseP, EF-G, and a ribosomal protein S5 share this peculiar topology, this domain has been suggested to be evolved from a common RNA-binding ancestor in the primordial translational apparatus (Stams et al., 1998). MutL and DNA gyrase are clearly not involved in protein biosynthesis, and this unusual fold is thus not specific for RNA binding only.

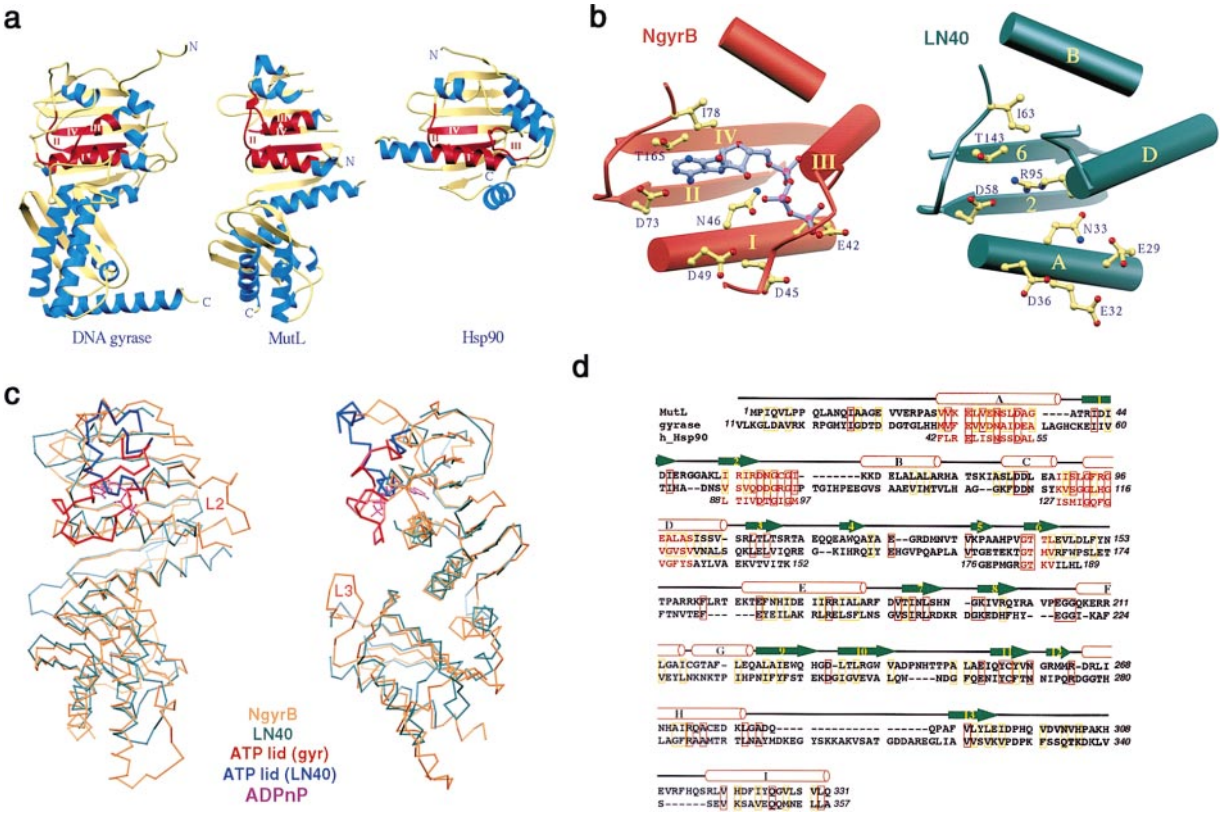

Figure 4. Structural Comparison of LN40, NgyrB, and Hsp90

(a) Ribbon diagrams of NgyrB, LN40, and human Hsp90 (PDB accession number: 1YET). The four conserved ATP-binding motifs are highlighted in red.

(b) Structural elements that form the ATP-binding site in NgyrB and LN40. Helices are represented as cylinders, strands as arrows. The four ATP-binding motifs are labeled in NgyrB. ADPnP, side chains that contributed to ADPnP binding in NgyrB, and their counterparts in LN40 are shown in ball-and-stick.

(c) Orthogonal views of overlay of the Cα traces of LN40 and NgyrB. Residues at the N and C termini of NgyrB are omitted for clarity. The regions in NgyrB that are equivalent to the L2 and L3 loops in LN40 are labeled.

(d) Structure-based sequence alignment of MutL and NgyrB. Identical sequences are outlined in red; conserved changed are outlined in yellow. The four ATP-binding motifs from human HSP90 are also included. The secondary structures of LN40 are shown above the sequence alignment.

MutL Is an ATPase

Before the crystal structure of LN40 was determined and MutL was found to be similar to NgyrB and Hsp90, we were surprised by the observation that MutL alone could activate MutH to cleave Mis-110 in an ATP-dependent manner (Figure 2c). No stimulation of DNA cleavage by MutL was observed under similar conditions without ATP (data not shown). We thus suspected that MutL might be an ATPase and assayed its ATPase activity. Incubation of α-^{32}P-labeled ATP with MutL resulted in the hydrolysis of ATP to ADP and Pi (Figure 6a). LN40 has no detectable ATPase activity (Figure 6a) despite the overall structural similarity to NgyrB and its ability to bind ATP. We suspect that the C-terminal region of MutL, either directly or by promoting dimer formation, provides additional elements for ATP hydrolysis. The C-terminal region may also help to reorient the two domains in LN40 to a conformation competent for ATP hydrolysis. Using ATP as a substrate, the Km of MutL is $\sim$90 μM and kcat is 0.4/min at pH 8.0 and 37°C (Figure 6b). The slow ATP hydrolysis rate allowed the detection of ATP binding as shown earlier.

The ATPase activity of MutL is consistent with the structural similarity of LN40 to NgyrB and Hsp90. We further tested the functional similarity of the ATPase active site using a gyrase inhibitor, novobiocin. Novobiocin is an antibiotic derived from coumarins that specifically inhibits the ATPase activity of DNA gyrase at nanomolar concentrations. The crystal structure of the first domain of NgyrB complexed with novobiocin shows that novobiocin inhibits the ATPase activity of DNA gyrase by partially occupying the ATP-binding site (Lewis et al., 1996). We found that novobiocin can inhibit the ATPase activity of MutL with a Ki of $\sim$0.25 mM (Figure 6c). Activation of MutH by MutL is also inhibited by novobiocin with a similar Ki (data not shown). Binding of novobiocin to MutL is much weaker than to DNA gyrase, which is probably due to the $>$60% sequence difference between the two proteins. Nevertheless, this novobiocin inhibition strengthens the notion that MutL is an authentic ATPase.

It was reported previously that trace amounts of ATPase activity associated with MutL (98% pure) resulted from contamination with DNA helicase II (Grilley

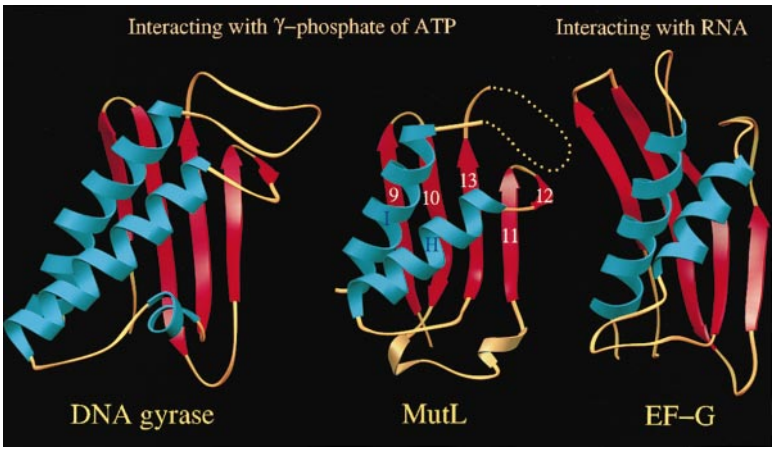

Figure 5. Ribbon Diagram of a Structurally Similar Domain in MutL, DNA Gyrase, and EF-G

et al., 1989; Yamaguchi et al., 1998). We have purified a His-tagged MutL to >99% purity and find that the ATPase activity repeatedly coelutes with MutL from a Sephadex-200 gel filtration column. If present, the 82 kDa helicase II should be separated from the 140 kDa MutL over the Sephadex-200 column unless they are associated specifically. Another potential source of contamination could be MutS, an ATPase known to be associated with MutL. However, the ATPase activities of MutL and MutS respond differently to heteroduplex DNA. Addition of Mis-110 at a DNA to protein molar ratio of 1:3 increases the ATP hydrolysis rate by MutS, but does not alter the ATPase activity of MutL (Figure 6a). The ATPase activity of MutL can be stimulated only at a DNA to protein ratio higher than 2:1 (data not shown). This difference helps to rule out the possibility of MutS contamination.

To prove that the detected ATPase activity is intrinsic to MutL, a point mutation in MutL designed to eliminate ATP hydrolysis was made. Based on structural homology between NgyrB and LN40, Glu-29 of MutL is likely to serve as a general base and activate the attacking water molecule to hydrolyze ATP. A MutL mutant, E29A, was constructed and purified in the same way as the native protein (manuscript in preparation). Based on UV absorption of purified protein-nucleotide complex, the E29A MutL can bind ATP and the ratio of nucleotide to protein is 0.6:1, similar to that of the ADP-MutL complex. As predicted, the E29A MutL is completely inactive in ATP hydrolysis (data not shown).

Combining the evidence presented, we conclude that MutL is an authentic ATPase. It is quite possible that the ATPase activity of MutL is regulated by other factors or proteins. There is also a slight chance that the presence of a histidine tag may enhance MutL ATPase activity. Conclusions concerning whether MutL functions as an independent ATPase in vivo and what may influence the ATPase activity await future experiments.

MutH Activation by MutL Depends on ATP Binding

The observation that in the presence of ATP MutL alone can activate the endonuclease activity of MutH (Figure 2c) seems difficult to reconcile with the fact that all three proteins, MutS, MutL, and MutH, are required for initiation of DNA mismatch repair (Lahue et al., 1989; Au et al., 1992). However, in previous studies the requirement of both MutS and MutL for MutH activation was determined in assays of mismatch repair, in which a mismatch site was ~1000 base pairs away from the MutH cleavage site (GATC sequence) on a ~6 kb DNA substrate (Au et al., 1992). To activate MutH, MutS and MutL therefore had to translocate over a long distance on the DNA. It is also reported (Au et al., 1992) that MutH activation is dependent on the distance between the mismatch and GATC sites, on whether the DNA substrate is circular or linear, and on the disposition of the mismatch and GATC sites relative to the DNA ends. In our assay, many of these problems are minimized by using a 110 bp DNA substrate in which the mismatch and GATC sites are separated by 63 bp so that little or

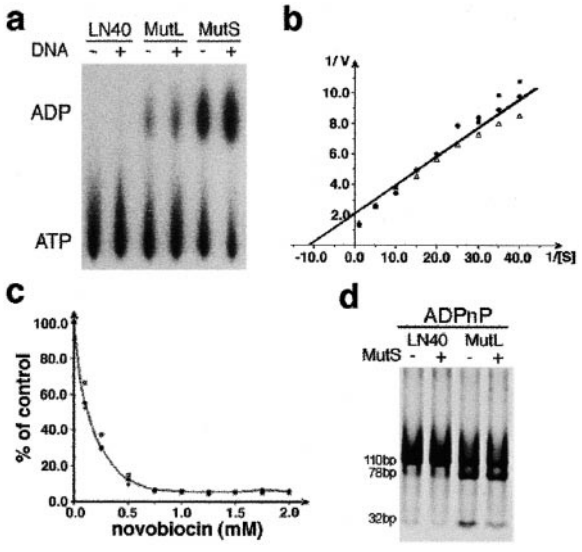

Figure 6. ATPase Activity of MutL

(a) ATPase assay of LN40, MutL, and MutS analyzed on a PEI-TLC plate. Addition of Mis-110 is indicated.

(b) A Lineweaver-Burk plot of the MutL ATPase activity. Three independent measurements of ATP hydrolysis at each ATP concentration (from 0.025 to 1 mM) are shown.

(c) Novobiocin inhibition of MutL ATPase activity. Three independent measurements are shown at each novobiocin concentration.

(d) Effect of ADPnP on MutH activation by LN40, MutL, and MutS.

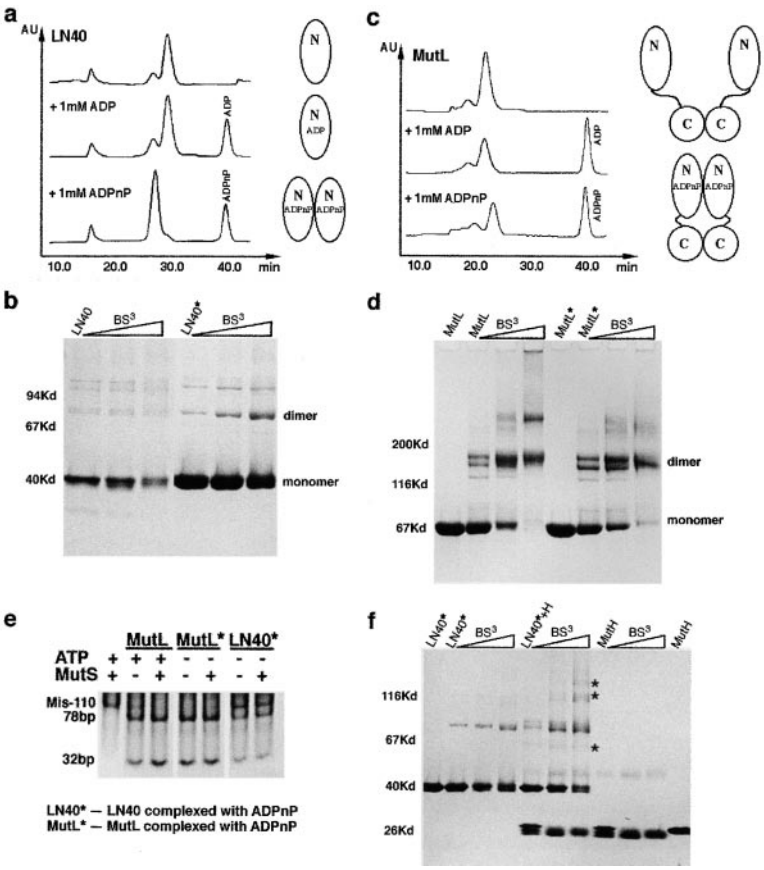

Figure 7. ADPnP-Induced Conformational Changes in LN40 and MutL

(a) Elution profiles from a Sephadex-200 column of LN40 and LN40 incubated with ADP or ADPnP.

(b) SDS gel of cross-linked LN40 and LN40 complexed with ADPnP (LN40*) with increasing concentration of BS^3.

(c) Elution profiles of MutL and MutL incubated with ADP or ADPnP.

(d) SDS gel of cross-linked MutL and MutL complexed with ADPnP (MutL*). The proposed conformational changes induced by ADPnP binding are diagrammed next to the elution profiles of LN40 and MutL.

(e) Cleavage of Mis-110 by MutH can be activated by purified MutL-ADPnP (MutL*) as well as ADPnP-LN40 (LN40*).

(f) SDS gel of cross-linked LN40-ADPnP complex (LN40*), LN40* with MutH and MutH alone by BS^3 in the presence of Mis-110. The bands that appear only in the LN40* and MutH mixture are labeled by stars.

no DNA translocation is needed. By using a ~50 times shorter DNA substrate, we greatly increase the effective substrate concentration. In addition, we increased both the protein and DNA concentrations in the reaction by ~1000-fold compared with Au et al. (1992). The fact that MutH activation by MutL is detected only at the higher concentrations of both DNA and proteins indicates weak interactions and possibly a high Km. The low concentration of MutL in vivo ensures that MutH will only be activated when MutS detects a mismatch.

The ATP-dependent MutH activation by MutL or by MutL and MutS was further tested with a nonhydrolyzable ATP analog, ADPnP. ADPnP can support MutL to activate MutH as well as or even better than ATP (Figure 6d). However, addition of MutS in the presence of ADPnP reduces the MutH activation (Figure 6d) rather than further stimulating it as observed in the presence of ATP (Figure 2c). We conclude that there are two ATP-dependent processes in mismatch-dependent activation of MutH. ATP binding, but not hydrolysis, is required for MutL to activate MutH. ATP hydrolysis, however, is required for full mismatch-dependent activation of MutH mediated by MutS and MutL, perhaps for MutS and MutL to translocate along DNA to the MutH cleavage site.

Conformational Changes Induced by ATP Binding

ATP and GTP are utilized in many biological systems. A common theme among these ATP- or GTP-dependent proteins is that they undergo conformational changes upon nucleotide binding and hydrolysis. These conformation changes, either directly or indirectly, switch on and off interactions with "effector" molecules (Vale, 1996). MutL, in addition to interacting with DNA, MutH, and MutS, has recently been shown to interact with helicase and VSR endonuclease (Drotschmann et al., 1998; Hall et al., 1998). The state of nucleotide that is associated with MutL may direct these protein–protein interactions.

Binding of ADPnP to LN40 induces a transition of LN40 from monomer to dimer as judged by size-exclusion chromatography and protein cross-linking assays (Figures 7a and 7b). Binding of ADPnP to the dimeric full-length MutL, however, results in a shift of elution profile of MutL from a Sephadex-200 column toward an apparently lower molecular weight (Figure 7c). The dimeric form of MutL has previously been established by its sedimentation coefficient (Grilley et al., 1989). While the molecular weight of dimeric MutL is less than 150 kDa, its elution profile from a size-exclusion column matches that of a 300 kDa globular protein, indicating that the MutL dimer is nonglobular. MutL complexed with ADPnP elutes from the Sephadex-200 at the same position as a globular protein of MW ~180 kDa. In addition, the MutL-ADPnP complex seems to be more stable in solution than MutL alone, which tends to aggregate. Results from protein cross-linking analyses show that incubation with ADPnP does not change the multimerization

state of MutL (Figure 7d). We, therefore, interpret this change in the elution profile of MutL from the size-exclusion column to be the result of a nucleotide-induced interaction of the N-terminal region (Figure 7c).

The ADPnP-induced conformational changes in MutL occur within minutes at protein concentrations between 0.3 to 2 mg/ml, while it takes hours for LN40 to fully dimerize at a similar concentration (data not shown). The MutL-ADPnP complex is exceedingly stable and can withstand 5 mM EDTA, whereas the LN40-ADPnP complex gradually dissociates and LN40 becomes monomeric (data not shown). These differences are likely due to MutL already being dimerized at the C-terminal region. After incubation with ADP, neither LN40 nor MutL show detectable change in their elution profiles from the sizing column (Figure 7), indicating dimerization and other conformational changes are specifically induced by ATP binding.

The ADPnP-induced dimerization of LN40 and conformational change of MutL are supported by the MutH activation assay. Purified LN40-ADPnP complex can activate MutH to cleave Mis-110, as does purified MutL-ADPnP complex (Figure 7e). Thus, we conclude that ADPnP induces similar conformational changes in LN40 and MutL and that such conformational changes are sufficient to activate MutH. ATP-dependent activation of MutH by MutL is likely due to the direct interactions between MutH and MutL and not due to non-sequence-specific and ATP-independent DNA binding by MutL. Cross-linking of MutH and LN40-ADPnP complex in the presence of Mis-110 DNA at a molar ratio of 1:1:1 gives rise to new protein bands in SDS gels, which are not observed when either MutH or LN40-ADPnP is cross-linked in the presence of the same DNA (Figure 7f). The cross-linking results support that the dimeric form of LN40 and MutH physically interact.

A dimer of LN40 has been observed in the crystal structure. Two LN40 molecules were packed in each asymmetric unit with the eight-stranded β sheet back-to-back and ATP-binding pockets facing opposite. Although similar packing was also observed in yeast Hsp90 (Prodromou et al., 1997a), there is no indication of functional relevance for this crystallographic dimer of LN40. Interestingly, NgyrB undergoes a transition from monomer to dimer when incubated with ADPnP. The two subunits of the NgyrB-ADPnP complex exchange their N-terminal peptides, where the first 16 residues extend from one subunit to the next and contact the ADPnP bound to the second subunit (Wigley et al., 1991). In the absence of ATP or ATP analog, the same fragment of DNA gyrase remains monomeric.

Three disordered loops in addition to the ATP lid in LN40 are populated with conserved residues (Figure 1) and may play roles as conformational switches. The first loop (L1) consists of the N-terminal 19 residues. Studies of an LN40 mutant with the first 13 residues deleted show that L1 affects DNA binding, ADPnP-induced dimerization, and MutH activation (unpublished data). The results from the N-terminal deletion of LN40 and the overall similarity between MutL and DNA gyrase suggest the possibility that the dimer of LN40 induced by ADPnP is similar to that of NgyrB. The second flexible yet conserved loop (L2) is formed between strand 6 and helix E and is adjacent to L1. The third such loop (L3) is between strand β13 and helix I and is structurally equivalent to the loop that interacts with the γ-phosphate in NgyrB. The conformational changes in LN40 and MutL induced by ADPnP correlate well with their functions in activating MutH. We therefore postulate that the lid of the ATP pocket and L3 loop may be primary switches that directly interact with both the nucleotide and other repair proteins. L1 and L2 loops may become ordered and serve as contacting surfaces after primary conformational changes, such as dimerization of LN40 or relative rotation of the first and second domains, triggered by a bound ATP.

Molecular Basis for Defective *E. coli* MutL and Human MLH1

Based on the functional importance of the ATPase activity in the MutL family, it is not surprising to find that the majority of the defective mutations in *E. coli* MutL and in human MLH1 affect the ATP-binding site. Eleven out of eighteen mutations in the N-terminal region that render MutL a dominant mutator (Aronshtam and Marinus, 1996) occur among the conserved residues in the ATP-binding motifs. They are E29K, E32K, A37T, D58N, G60S, G93D, R95C, G96S, G96D, and S112L. Four of the remaining seven mutations, A16T, A16V, P305L, and H308Y, are on the L1 and L3 loops surrounding the ATP-binding site, and G238D probably disrupts the interface between the two domains in LN40. The last two mutations, S106F and A271V, may indirectly affect the ATP binding by altering the MutL structure. Most of the mutations in the C-terminal region of MutL that display dominant mutator phenotype are various truncations (Aronshtam and Marinus, 1996). While the N-terminal region is sufficient for MutL to interact with DNA, MutS, and MutH, the level of MutH activation by MutL may depend on the C-terminal region as discussed earlier. The C-terminal region has also been shown to physically interact with UvrD (Hall et al., 1998).

In the case of human MLH1, 9 out of 14 missense mutations found in the conserved N-terminal region in reported HNPCC cases (Peltomäki and Vasen, 1997) are located in and around the ATP-binding pocket (Figure 1). These mutations are P28L, M35R, S44F, G67R, I68N, I107R, T117R, T117M, and R265H. Two other mutations, V185G and G244D, are located on the domain interface, as is the G238D mutation of *E. coli* MutL. Some of these mutations probably directly affect ATP binding and hydrolysis, while the others are likely to alter the structure of the ATP-binding site.

Conclusions

It is intriguing that both MutS and MutL are ATPases. With a rather slow hydrolysis rate of ATP, MutL may be a molecular timer that allows orderly recruitment of endonuclease, single-strand binding protein and helicase to the repair machinery. It is also possible that MutL is a secondary motor protein that assists MutS to translocate along supercoiled DNA until a GATC site is found. The crystal structure of LN40 and the discovery

of the ATPase activity of MutL start to unveil the functions of the MutL family. In addition, we have shown that binding of ATP induces interactions of the N-terminal region of MutL and such conformational changes are sufficient for MutL or LN40 to activate MutH. Based on these findings, we propose that MutL utilizes ATP to regulate interactions among MutS, MutH, and UvrD and to coordinate stepwise events in DNA mismatch repair. The ATP-binding pocket in both DNA gyrase and Hsp90 also provides the binding sites for antibiotics and antitumor agents. The structural similarity among MutL, DNA gyrase, and Hsp90 provides a note of caution. Antibiotics that are intended for DNA gyrase or Hsp90 may also bind to MutL and its homologs and therefore may hinder DNA repair as a side effect. The differential binding of novobiocin to DNA gyrase and MutL, however, is an example that specific inhibition can be accomplished. The results of structural and functional studies reported here provide a glimpse of the operation of DNA repair machinery. Ultimately, information obtained from MutL and future studies on human homologs will contribute to the understanding of mutagenesis and prevention of cancers.

Experimental Procedures

Protein Purification and Crystallization

His-tagged *E. coli* MutL was overexpressed in BL21 cells containing plasmid pTX418 and purified over a Ni column as described (Feng and Winkler, 1995). When treated with thrombin to remove the His-tag, MutL was cleaved to a 40 kDa (LN40) and a 30 kDa (L30) fragments. These two fragments were isolated with a mono-Q column. LN40 was further purified with a Superdex-75 column and concentrated to 7 mg/ml in 20 mM Tris (pH 8.4), 150 mM KCl, 1 mM EDTA, 1 mM DTT, and 5% glycerol. N-terminal sequencing of each fragment indicated that LN40 contains residues 1–349 with three additional residues left from the His-tag and LC30 contains residues 350–615. Size-exclusion chromatography, dynamic light scattering, and equilibrium ultracentrifugation showed that LN40 was monomeric in solution.

Crystals of LN40 were grown at 20°C using the hanging drop diffusion method. The precipitant buffer contained 100 mM bis-Tris propane (pH 6.6), 100 mM Mg acetate, 100 mM $MgSO_4$, 2 mM DTT, and 20% PEG 8000. Crystals appeared over a period of 3–4 days and reached the maximum size of 0.1 × 0.1 × 0.3 mm in 2 weeks. These crystals belonged to space group $I2_12_12_1$ (Table 1). There were two molecules in each asymmetric unit and 57% (v/v) solvent. LN40 crystals were stabilized in the mother liquor with final concentration of PEG 8000 at 35% and an addition of 5% ethylene glycol as cryo-solvent. A mercury derivative was obtained by soaking LN40 crystals in the stabilization solution with 0.6 mM ethyl-mercury phosphate (EMP) for a day. Immediately before flash freezing, LN40 crystals were successively transferred to stabilization buffers with 10% and 20% ethylene glycol.

Data Collection and Structure Determination

Diffraction data were collected at 90°K on an R axis IPII detector mounted on a Rigaku RU200 generator and processed using DENZO, SCALEPACK, and CCP4 (CCP4, 1994; Otwinowski and Minor, 1997). Although cell constants did not change very much (Table 1), LN40 crystals were nevertheless not isomorphous even among native ones. We had to screen a number of complete datasets based on R_{iso} and Patterson map in order to get an isomorphous pair of native and derivative data. Two Hg sites were readily located in Harker sections. SHELX (Sheldrick and Schneider, 1997) was used to determine the origin because the cross vectors were very close to 0.25 along each of three axes. Successive rounds of Difference Fourier search led to three more minor sites of Hg. These five Hg sites were refined using MLPHARE (CCP4, 1994). The calculated electron density map showed a clear solvent boundary. After solvent flattening by DM (CCP4, 1994), many helices and β strands were obvious. The map was further improved by noncrystallographic 2-fold averaging using MAMA (Kleywegt and Jones, 1994) and DM. The resulting map showed a clear trace of the polypeptide chain. However, there were a number of breaks along the main chain and part of the first domain had very weak densities for side chain atoms, which made the sequence assignment difficult. Using phase combination after partial structure refinement and common sense of protein chemistry, residues 20 to 331 excluding four disordered loops (residues 74 to 79, 126 to 131, 150 to 162, and 300 to 312) were confidently traced using O (Jones et al., 1991). The current model is refined to 2.9 Å with noncrystallographic restraint using X-PLOR (Brünger, 1992) (Table 1). All residues but one (99.7%) are in the "most favorable" and "additional allowed" regions in a Ramachandran plot. The one exceptional residue is in a "generously allowed" region. Analysis by PROCHECK ranks the structure to be as good as or better than the average quality of structures refined at 2.9 Å.

DNA Cleavage Assay

E. coli MutS, MutL, and MutH were separately expressed as described (Feng and Winkler, 1995). Each protein was purified over a Ni column. MutL was further purified over a monoQ and a Superdex-200 column. MutH was purified as described (Ban and Yang, 1998). Each of the proteins was exchanged into Buffer B (20 mM Tris, 300 mM KCl, 0.1 mM EDTA, 1 mM DTT, and 5% glycerol) over a small desalting column and concentrated to 100–200 μM. The 110 bp DNA heteroduplex (Mis-110) was annealed from two chemically synthesized oligonucleotides, which were purified by reverse-phase chromatography. DNA was stored in Tris-EDTA buffer at 80 μM concentration. Immediately prior to cleavage assays, each protein was diluted to 4 μM in buffer A (20 mM Tris, 30 mM KCl, 5 mM $MgCl_2$, 1 mM DTT) with no additives, 1 mM ATP or 1 mM ADPnP, and DNA was diluted to 2 μM in the same buffer. Eight picomoles each of MutH and MutS, 12 pmol of MutL or LN40, and 2 pmol of the heteroduplex DNA were mixed with the dilution buffer to a final volume of 15 μl. Cleavage reactions were incubated at 20°C for 3 hr and stopped by addition of 0.17% SDS. Cleavage products were analyzed on a 10% polyacrylamide gel by electrophoresis in TBE buffer at 180 V for 40 min. DNA was stained with SYBR-green.

DNA Mobility Shift Assay

Hetero- or homoduplex DNA (4 pmol) was incubated with 4, 12, and 20 pmol of LN40 in 15 μl buffer A for 2 hr. The reaction mix (12 μl) was analyzed on a 6% polyacrylamide gel by electrophoresis in TBE buffer at 80 V for 2 hr. Gels were stained in SYBR-green and photographed. A 72 bp homoduplex with blunt ends, OE-72, is cleaved from plasmids produced in vivo.

Nucleotide-Binding Assay

LN40 or MutL (1–2 mg/ml) in buffer B plus 5 mM $MgCl_2$ was incubated with 1mM ADP, ATP, or ADPnP at room temperature for 1 hr and then 4°C overnight. The protein-nucleotide mixture (100 μl) was injected into a preequilibrated Sephadex-200 column (Pharmacia-LKB) and eluted at a flow rate of 0.5 ml/min with the same buffer.

The nucleotide to protein ratio (x:1) is obtained using the formula $x = (k*Ep280 - Ep260) / (En260 - k*En280)$, in which k is the UV absorption ratio of the protein-nucleotide complex at 260 nm versus 280 nm; Ep280 and Ep260 are the molar extinction coefficients of protein (54,200 and 27,100 for MutL; 26,500 and 20,900 for LN40); En280 and En260 are of the nucleotides (2,200 and 13,600, respectively).

ATPase Assay

MutS or MutL (12 pmol) were incubated with 750 pmol of α-^{32}P-labeled ATP in 15 μl solution of buffer A at 37°C for 30 min. The effect of heteroduplex DNA on ATPase activity was assayed by addition of 4 pmol of DNA in the reaction mix. One microliter of each reaction mix was spotted on a PEI-TLC plate. Labeled ATP and ADP were separated by developing the TLC plate in 1 M formic acid and 0.4 M $LiCl_2$ and detected on a phosphor imaging plate.

Kinetic data of ATP hydrolysis were obtained at three MutL concentrations (0.7, 1.2, and 2 μM) with ATP concentrations varying from 25 μM to 1 mM. Km and kcat were derived from a double reciprocal Lineweaver-Burk plot. Novobiocin inhibition was tested with novobiocin concentrations varying from 0.1 to 2 mM in the reaction mixture of 1.2 μM MutL and 80 μM of α-^{32}P-labeled ATP.

Protein Cross-Linking by BS^3

LN40, LN40-ADPnP complex (LN40*), MutL, and MutL-ADPnP complex (MutL*) at 10 μm concentrations were incubated with 0.11, 0.33, and 1 mM BS^3 (Bis-sulfosuccinimidyl suberate) in buffer A and 100 mM KCl for 1 hr at 22°C. Ten microliters of each cross-linked sample was mixed with SDS sample buffer and analyzed by electrophoresis on 4%–12% or 4%–20% SDS gels. Cross-linking of MutH and LN40* was carried out in the presence of Mis-110 DNA. MutH, LN40* (12 μM) or MutH and LN40* (12 μM each) were mixed with 12 μM Mis-110 in buffer A and cross-linked by 0.11, 0.33, and 1 mM BS^3 at 22°C for 1 hr. Cross-linked samples were analyzed by eletrophoresis on a 4%–12% SDS gel and stained with Coomassie blue.

Sequence and Structure Comparisons

Sequences of the MutL family were aligned based on the LN40 structure. Structures of NgyrB, Hsp90, and LN40 were superimposed manually; the superposition was then best fitted using the least-square method. Structural figures were generated using RIBBONS (Carson, 1987) except Figure 3c, which was generated using GRASP (Nicholls et al., 1991).

Acknowledgments

We thank G. Feng and M. Winkler for the MutS, L, and H expression vectors; J. Wang and J. Tormo for helpful discussions on structure determination; M. Junop and E. Deye for the E29A mutant; I. Biswas for help with ATPase assay; M. O'Dea for novobiocin; R. Ghirlando for ultracentrifugation analysis; D. Wigley for the coordinates of NgyrB and stimulating discussions; B. Craigie, M. Gellert, W. Hendrickson, M. Junop, D. Leahy, and K. Mizuuchi for comments and suggestions on the manuscript. Correspondence and request for materials should be addressed to W. Y. (Wei.Yang@nih.gov).

Received June 5, 1998; revised September 10, 1998.

References

Ævarsson, A., Brazhnikov, E., Garber, M., Zheltonosova, J., Chirgadze, Y., Al-karadaghi, S., Svensson, L.A., and Lilhas, A. (1994). Three-dimensional structure of the ribosomal translocase: elongation factor G from Thermus thermophilus. EMBO J. *13*, 3669–3677.

Allen, D.J., Makhov, A., Grilley, M., Taylor, J., Thresher, R., Modrich, P., and Griffith, J.D. (1997). MutS mediates heteroduplex loop formation by a translocation mechanism. EMBO J. *14*, 4467–4476.

Aronshtam, A., and Marinus, M.G. (1996). Dominant negative mutator mutations in the mutL gene of *Escherichia coli*. Nucleic Acids Res. *24*, 2498–2504.

Au, K.G., Welsh, K., and Modrich, P. (1992). Initiation of methyl-directed mismatch repair. J. Biol. Chem. *267*, 12142–12148.

Baker, S.M., Bronner, C.E., Zhang, I., Plug, W., Robatzek, M., Warren, G., Elliott, E.A., Yu, J., Ashley, T., Arnheim, N. et al. (1995). Male mice defective in the DNA mismatch repair gene PMS2 exhibit chromasome synapsis in meiosis. Cell *82*, 309–319.

Ban, C., and Yang, W. (1998). Structural basis for MutH activation in *E. coli* mismatch repair and relationship of MutH to restriction endonucleases. EMBO J. *17*, 1526–1534.

Bergerat, A., de Massy, B., Gadelle, D., Varoutas, P.-C., Nicolas, A., and Forterre, P. (1997). An atypical topoisomerase II from archaea with implications for meiotic recombination. Nature *386*, 414–417.

Brünger, A.T. (1992). X-PLOR, Version 3.1, A System for X-Ray Crystallography and NMR (New Haven, CT: Yale University Press).

Carson, M. (1987). Ribbon models of macromolecules. J. Mol. Graph. *5*, 103–106.

CCP4 (1994). The CCP4 suite: programs for protein crystallography. Acta Crystallogr. D *50*, 760–763.

Cooper, D.L., Lahue, R.S., and Modrich, P. (1993). Methyl-directed mismtach repair is bidirectional. J. Biol. Chem. *268*, 11823–11829.

Czworkowski, J., Wang, J., Steitz, T.A., and Moore, P.B. (1994). The crystal structure of elongation factor G complexed with GDP, at 2.7 Å resolution. EMBO J. *13*, 3661–3668.

Dao, V., and Modrich, P. (1998). Mismatch-, MutS-, MutL-, and helicase II-dependent unwinding from the single-strand break of an incised heteroduplex. J. Biol. Chem. *273*, 9202–9207.

de Wind, N., Dekker, M., Berns, A., Radman, M., and te Riele, H. (1995). Inactivation of the mouse Msh2 gene result in mismatch deficiency, methylation tolerance, hyperrecombination and predisposition to cancer. Cell *82*, 321–330.

Drotschmann, K., Aronshtam, A., Fritz, H.-J., and Marinus, M.G. (1998). The *Escherichia coli* MutL protein stimulates binding of Vsr and MutS to heteroduplex DNA. Nucleic Acids Res. *26*, 948–953.

Feng, G., and Winkler, M.E. (1995). Single-step purifications of His6-MutH, His6-MutL and His6-MutS repair proteins of *Escherichia coli* K-12. Biotechniques *19*, 956–965.

Grilley, M., Welsh, K.M., Su, S.-S., and Modrich, P. (1989). Isolation and characterization of the *Escherichia coli mutL* gene product. J. Biol. Chem. *264*, 1000–1004.

Grilley, M., Griffith, J., and Modrich, P. (1993). Bidirectional excision in methyl-directed mismatch repair. J. Biol. Chem. *268*, 11830–11837.

Hall, M.C., Jordan, J.R., and Matson, S.W. (1998). Evidence for a physical interaction between the *Escherichia coli* methyl-directed mismatch repair proteins MutL and UvrD. EMBO J. *17*, 1535–1541.

Hangaishi, A., Ogawa, S., Mini, K., Hosoya, N., Chiba, S., Yazaki, Y., and Hirai, H. (1997). Mutations and loss of expression of a mismatch repair gene, hMLH1, in leukemia and lymphoma cell lines. Blood *89*, 1740–1747.

Holm, L., and Sander, C. (1993). Dali: version 2.0. J. Mol. Biol. *233*, 123–138.

Jones, T.A., Zou, J.-Y., and Cowan, S.W. (1991). Improved methods for building models in electron density maps and the location of errors in these models. Acta Crystallogr. A *47*, 110–119.

Kleywegt, G.J., and Jones, T.A. (1994). Masks and bones in "From first map to final model." CCP4, 59–66.

Kolodner, R. (1996). Biochemistry and genetics of eukaryotic mismatch repair. Genes Dev. *10*, 1433–1442.

Kramer, W., Kramer, B., and Williamson, M.S. (1989). Cloning and sequence of DNA mismatch repair gene PMS1 from Saccharomyces cerevisiae: homology of PMS1 to prokaryotic MutL and HexB. J. Bacteriol. *171*, 5339–5346.

Lahue, R.S., Au, K.G., and Modrich, P. (1989). DNA mismatch correction in a defined system. Science *245*, 160–164.

Lewis, R.J., Singh, O.M., Smith, C.V., Skarzynski, T., Maxwell, A., Wonacott, A.J., and Wigley, D.B. (1996). The nature of inhibition of DNA gyrase by the coumarins and the cyclothialidines revealed by X-ray crystallography. EMBO J. *15*, 1412–1420.

Loeb, L.A., Springgate, C.F., and Battula, N. (1974). Errors in DNA replication as a basis of malignant changes. Cancer Res. *34*, 2311–2321.

Modrich, P. (1991). Mechanisms and biological effects of mismatch repair. Annu. Rev. Genet. *25*, 229–253.

Modrich, P., and Lahue, R. (1996). Mismatch repair in replication fidelity, genetic recombination, and cancer biology. Annu. Rev. Biochem. *65*, 101–133.

Mushegian, A.R., Bassett, Jr., D.E., Boguski, M.S., Bork, P., and Koonin, E.V. (1997). Positionally cloned human disease genes: patterns of evolutionary coservation and functional motifs. Proc. Natl. Acad. Sci. USA *94*, 5831–5836.

Nicholls, A., Sharp, K.A., and Honig, B. (1991). Protein folding and association: insights from the interfacial and themodynamic properties of hydrocarbons. Proteins Struct. Funct. Genet. *11*, 281–296.

Nowell, P.C. (1976). The clonal evolution of tumor cell populations. Science *194*, 23–28.

Otwinowski, Z., and Minor, W. (1997). Processing of X-ray diffraction data collected in oscillation mode. Methods Enzymol. *276*, 307–326.

Pang, Q., Prolla, T.A., and Liskay, M. (1997). Functional domains of the Saccharomyces cerevisiae Mlh1p and Pms1p DNA mismatch repair proteins and there relevance to human hereditary nonpolyposis colorectal cancer-associated mutations. Mol. Cell Biol. *17*, 4465–4473.

Peltomäki, P., and Vasen, H.F. (1997). Mutations predisposing to hereditary nonpolyposis colorectal cancer: database and results of a collaborative study. Gastroenterology *113*, 1146–1158.

Prodromou, C., Roe, S.M., O'Brien, R., Ladbury, J.E., Piper, P.W., and Pearl, L.H. (1997a). Identification and structural characterization of the ATP/ADP-binding site in the Hsp90 molecular chaperone. Cell *90*, 65–75.

Prodromou, C., Roe, S.M., Piper, P.W., and Pearl, L.H. (1997b). A molecular clamp in the crystal structure of the N-terminal domain of the yeast Hsp90 chaperone. Nat. Struct. Biol. *4*, 477–482.

Sheldrick, G.M., and Schneider, T.R. (1997). SHELX: high-resolution refinement. Methods Enzymol. *277*, 319–343.

Stams, T., Niranjanakumari S., Fierke, C., and Christianson, D.W. (1998). Ribonuclease P protein structure: evolutionary origins in the translational apparatus. Science *280*, 752–755.

Stebbins, C.E., Russo, A.A., Schneider, C., Rosen, N., Hartl, F.U., and Pavletich, N.P. (1997). Crystal structure of an Hsp90-geldanamycin complex: targeting of a protein chaperone by an antitumor agent. Cell *89*, 239–250.

Vale, R. (1996). Switches, latches, and amplifiers: common themes of G proteins and molecular motors. J. Cell Biol. *135*, 291–302.

Wigley, D.B., Davies, G.J., Dodson, E.J., Maxwell, A., and Dodson, G. (1991). Crystal structure of an N-terminal fragment of the DNA gyrase B protein. Nature *351*, 624–629.

Yamaguchi, M., Dao, V., and Modrich, P. (1998). MutS and MutL activate DNA helicase II in a mismatch-dependent manner. J. Biol. Chem. *273*, 9197–9201.

Brookhaven Protein Data Bank ID Code

Coordinates reported in this paper have been deposited in the Brookhaven Protein Data Bank with ID code of 1BKN.